Numerical simulation of turbulent flow and heat transfer in multi-channel, narrow-gap fuel element

Huang Jun, Wang Q.W. and Tao W.Q.
School of Energy and Power Engineering, Xi'an Jiaotong University, Xi'an, Shaanxi, PRC

Received June 2001
Accepted January 2002

Keywords *Turbulent flow, Heat transfer*

Abstract *A computational study of convective heat transfer for turbulent flows in multi-channel, narrow-gap fuel element has been carried out, using a general marching procedure. The fluid distribution adjustment among seven annular-sector channels is based on the assumption of the same pressure drop in these passages. It was found that the inlet velocities of the bilateral channels are lower than those of the middles, and the axial local heat transfer coefficients for the seven channels do not approach the fully developed constant value. At each cross section, the periphery temperature distribution is not uniform, while the local temperature distribution along axial coordinate is of sinuous type with the peak at x = 0.7–0.8 m. At the same Reynolds number, the averaged Nusselt numbers of water in Channel 1 and Channel 7 are higher than those in the middles. The maximum surface temperature increases almost linearly with the inlet water temperature, whereas it decreases almost asymptotically with the inlet average velocity.*

Notation

D = channel equivalent diameter, m
F = mass flow rate, kg/s
h = heat transfer coefficient, W/m^2.℃
l = mixing length
L = total length of the cooled channel, m
Nu = Nusselt number
p = pressure, Pa
$\tilde{p}$ = small pressure variation, Pa
$\bar{p}$ = space-average pressure over the cross section, Pa
Pr = Prandtl number
q = heat flux, W/m^2
r = radial distance; radial coordinate, m (Figure 1)
Re = Reynolds number
$r_{i,ic}$ = inner radial distance of the inner casing, m (Figure 1)
$r_{o,oc}$ = outer radial distance of the outer casing, m (Figure 1)
S_u, S_v, S_w = volumetric source term in x, r, θ momentum equation
t = temperature, ℃
u = axial velocity component, m/s
v = radial velocity component, m/s
w = angular velocity component, m/s
x = axial distance; axial coordinate
θ = angular distance; angular coordinate, rad
μ = fluid dynamics viscosity, kg/m.s
μ_t = turbulent viscosity, kg/m.s
μ_{eff} = equivalent fluid viscosity, $\mu + \mu_t$
σ_T = turbulent Prandtl number

This research work was supported by the National Natural Science Foundation of China (No. 59806011, 59995460-2).

Engineering Computations, Vol. 19 No. 3, 2002, pp. 327-345.

DOI 10.1108/02644400210423972

Δp = pressure drop for a channel
ϕ = the dependent variable ϕ

Superscripts
n = temporal solution to the difference equation at n_{th} step

Subscripts
i = inner
in = channel inlet locations
max = maximum

1. Introduction

In a high flux engineering test reactor (HFETR), the multi-channel, narrow-gap fuel element, with enriched uranium, is employed to meet the demand for high-performance. High-velocity, high-pressure water flows through seven narrow-gap annular channels between concentric fuel layers, each of which is of sandwich type consisted of two aluminum layers and a uranium one (Figure 1). Uranium layers generate enormous heat flux, uniform peripherally but sinuous axially, and are cooled by the high-pressure and high-velocity water. Each

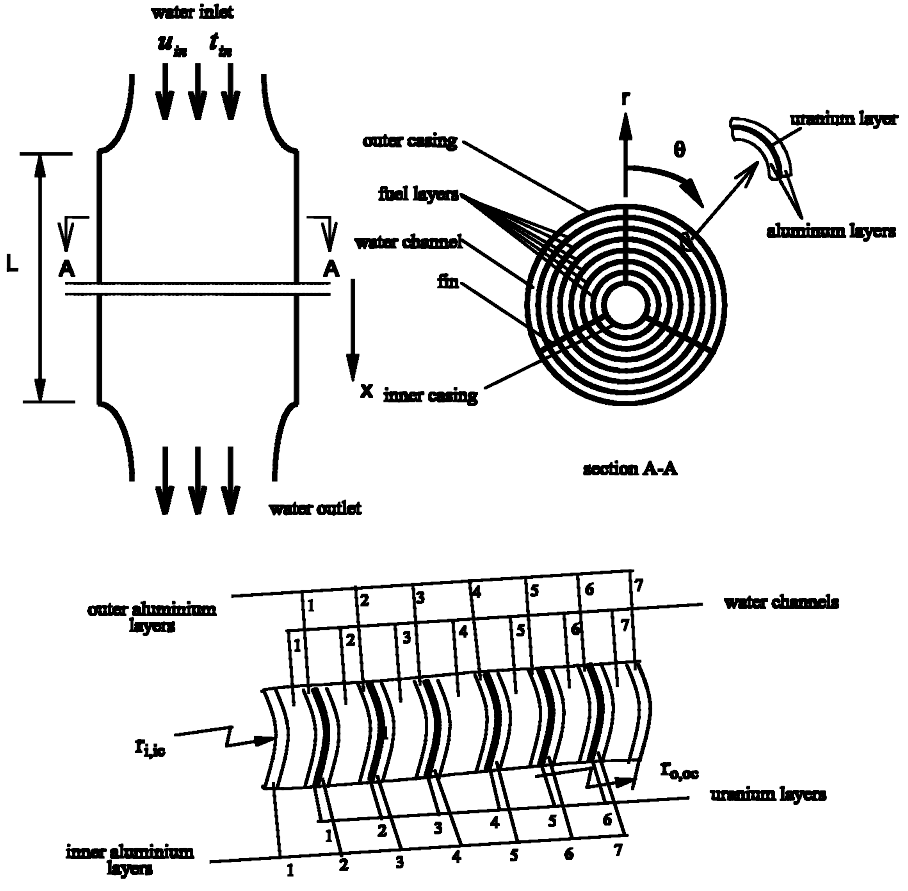

Figure 1.
Schematic diagram of the physical domain

water channel is separated by three fins along the peripheral, forming three annular-sector channels. To keep the reactor operating safely, the maximum surface temperature for the channels in the fuel element should not surpass the designed value. It is, therefore, of great practical importance to investigate the temperature distribution in this kind of fuel element.

Some researches have been conducted to investigate turbulent flow and heat transfer in the fuel element, experimentally or theoretically. Due to the extremely high price, and more importantly the difficulties to arrange thermocouples in the narrow channels, experimental data are very limited (Chen and Jiang, 1984). The numerical method is a useful alternative in this situation (Yu, 1981; Wang, 1981). In the works by Yu (1981) and Wang (1981), the fuel element was divided into several districts, and their temperature distributions were solved separately instead of solving the entire region. Many simplifying assumptions and empirical equations had to be employed to fill the coupling of the separated districts. These include:

(1) one-dimensional or two-dimensional conduction model was used for the fuel region;

(2) along the fuel layer element surface the convective heat transfer coefficients were determined from empirical equation;

(3) thermophysical properties were temperature-independent;

(4) the inlet velocities for the seven channels were assumed to be the same as each other.

All these assumptions made the accuracy of the numerical results quite questionable and far from satisfactory to give enough information for guiding the operation.

As mentioned earlier, annular-sector ducts are involved in this configuration. Although convective flow and heat transfer in annular-sector ducts has been performed by several authors (Lin *et al.*, 1995; Nida, 1980; Soliman, 1987; Sparrow *et al.*, 1964), no results are provided in the literature for multi-passage, annular-sector ducts subjected to a non-uniform heat flux. The key issues included in the numerical simulation of this problem are as follows:

(1) the flow distribution in different subchannels is unknown prior, rather, it should be determined during the computational procedure with a given total flow flux;

(2) the conduction in the fuel layer and the convection of the water channels surface are coupled, making the problem of conjugated type;

(3) the variation of the fluid thermophysical properties should be taken into account because of high heat flux released by the fuel layer.

The objective of this article is to develop a three-dimensional, marching calculation procedure mathematical modeling for the fuel element, which includes

seven narrow-gap passages, six uranium layers and fourteen aluminum layers, as schematically shown in Figure 1. The fluid distribution among passages is adjusted during the simulation procedure so as to guarantee the same pressure drop between the inlets and outlets of each channels. Some thermophysical properties of water, such as viscosity and Prandtl number, are considered to be temperature-dependent. In such kind of the peculiar structure of the channels, no recirculating flow in the axial direction may be expected and the flow is mainly of parabolic type. Therefore, a three-dimensional parabolic model is selected to simulate the flow procedure. Although various sophisticated turbulence models have been developed (Hanjalic, 1994; Ramdhyani, 1997), the mixing length theory is considered as the right choice for the present simulation. A parametrical study is also conducted, where the effects of the inlet water temperature and velocity are examined.

2. Mathematical model

As sketched in Figure 1, six ring-like fuel layers and inner and outer casings are assembled concentrically with fins used as spacings to fix their position. Each fuel layer consists of three layers. The middle one is uranium, the generator of heat flux, while the bilateral layers are aluminum. The inner casing, the outer casing and fins are also made of aluminum. High-velocity, high-pressure water flows through the seven narrow-gap annular gaps, keeping the system in the desired temperature. It is assumed that the flow is steady, turbulent and incompressible with temperature-dependent thermoproperties. The physical properties of uranium and aluminum are supposed to be constant because they almost have no change in the range of temperature studied. Heat flux generated by uranium layers is uniform peripherally (θ) but sinuous axially (x) (Figure 1), which could be expressed by:

$$q(x) = q_{\max} \cdot \sin\left(\frac{\pi(100x + 9)}{118}\right) \tag{1}$$

where x is the axial distance. The thermal conductivities of aluminum and uranium are 200.7 W/m.°C and 168.9 W/m.°C, while their densities are 2700 kg/m^3 and 5060 kg/m^3 respectively. The thickness of both the uranium and the aluminum of each fuel layer are 0.5 mm. The total length of the cooled channels is one meter. The outer diameter D_o and the inner diameter D_i of each fuel layer and the inner and outer casings are listed in Table I. It should be noted that the number system in Table I was also shown in Figure 1.

Considering the symmetry of the present problem, only one-third of the fuel element needs to be taken into account (that is, $\theta = 2\pi/3$, Figure 1). In this flow problem there exists a predominant direction of flow (the axial direction, x) in which upwind convective flow greatly influences the downwind, thus it can be treated as parabolic in the streamwise direction, therefore the streamwise

diffusion of momentum and energy can be omitted (Patankar and Spalding, 1972).

The control volume based, fully implicit, finite difference method was applied to solve the flow of the channels in the present work (Patankar and Spalding, 1972). The governing equations for the flow and thermal fields may be written as:

Continuity:

$$\frac{\partial u}{\partial x} + \frac{1}{r}\frac{\partial w}{\partial \theta} + \frac{\partial v}{\partial r} + \frac{v}{r} = 0 \tag{2}$$

Momentum:

$$\frac{\partial}{\partial x}(\rho u^2) + \frac{1}{r}\frac{\partial}{\partial r}(r\rho uv) + \frac{1}{r}\frac{\partial}{\partial \theta}(\rho uw) = \frac{1}{r}\frac{\partial}{\partial r}\left(\mu_{\text{eff}} r \frac{\partial u}{\partial r}\right) + \frac{1}{r}\frac{\partial}{\partial \theta}\left(\frac{\mu_{\text{eff}}}{r}\frac{\partial u}{\partial \theta}\right) + S_u \tag{3a}$$

$$\frac{\partial}{\partial x}(\rho uv) + \frac{1}{r}\frac{\partial}{\partial r}(r\rho v^2) + \frac{1}{r}\frac{\partial}{\partial \theta}(\rho vw) = \frac{1}{r}\frac{\partial}{\partial r}\left(\mu_{\text{eff}} r \frac{\partial v}{\partial r}\right) + \frac{1}{r}\frac{\partial}{\partial \theta}\left(\frac{\mu_{\text{eff}}}{r}\frac{\partial v}{\partial \theta}\right) + S_v \tag{3b}$$

$$\frac{\partial}{\partial x}(\rho uw) + \frac{1}{r}\frac{\partial}{\partial r}(r\rho vw) + \frac{1}{r}\frac{\partial}{\partial \theta}(\rho w^2) = \frac{1}{r}\frac{\partial}{\partial r}\left(\mu_{\text{eff}} r \frac{\partial w}{\partial r}\right) + \frac{1}{r}\frac{\partial}{\partial \theta}\left(\frac{\mu_{\text{eff}}}{r}\frac{\partial w}{\partial \theta}\right) + S_w \tag{3c}$$

where S_u, S_v, S_w are the volumetric source terms defined as

$$S_u = -\frac{\partial \tilde{p}}{\partial x} + \frac{1}{r}\frac{\partial}{\partial r}\left(r\mu_{\text{eff}}\frac{\partial v}{\partial x}\right) + \frac{1}{r}\frac{\partial}{\partial \theta}\left(\mu_{\text{eff}}\frac{\partial w}{\partial x}\right) \tag{4a}$$

$$S_v = -\frac{\partial \tilde{p}}{\partial r} + \frac{\partial}{\partial x}\left(\mu_{\text{eff}}\frac{\partial u}{\partial r}\right) + \frac{1}{r}\frac{\partial}{\partial r}\left(r\mu_{\text{eff}}\frac{\partial v}{\partial r}\right) + \frac{1}{r}\frac{\partial}{\partial \theta}\left(\mu_{\text{eff}}\frac{\partial (w/r)}{\partial \theta}\right) - \frac{2\mu_{\text{eff}}}{r}\left(\frac{1}{r}\frac{\partial w}{\partial \theta} + \frac{v}{r}\right) + \frac{\rho w^2}{r} \tag{4b}$$

$$S_w = -\frac{1}{r}\frac{\partial \tilde{p}}{\partial \theta} + \frac{\partial}{\partial x}\left(\mu_{\text{eff}}\frac{\partial u}{r\partial \theta}\right) + \frac{1}{r}\frac{\partial}{\partial r}\left(r\mu_{\text{eff}}\left(\frac{1}{r}\frac{\partial v}{\partial \theta} - \frac{w}{r}\right)\right) \tag{4c}$$

	Inner casing	Fuel layers No. 1	No. 2	No. 3	No. 4	No. 5	No. 6	Outer casing
D_o (mm)	14	21	28	35	42	49	56	63
D_i (mm)	12	18	25	32	39	46	53	60

Table I.
Value of D_o and D_i for six fuel layers and the inner and outer casings

Energy:

$$\frac{\partial}{\partial x}(\rho ut) + \frac{1}{r}\frac{\partial}{\partial r}(r\rho vt) + \frac{1}{r}\frac{\partial}{\partial \theta}(\rho wt) = \frac{1}{r}\frac{\partial}{\partial r}\left(r(\mu/\mathrm{Pr} + \mu_t/\sigma_T)\frac{\partial t}{\partial r}\right) + \frac{1}{r}\frac{\partial}{\partial \theta}\left(\frac{\mu/\mathrm{Pr} + \mu_t/\sigma_T}{r}\frac{\partial t}{\partial \theta}\right) \quad (5)$$

where $\mu_{\mathrm{eff}} = \mu + \mu_t$, $\sigma_T = 0.9$, $\mu_t = \rho l^2 |\partial u/\partial y|$.

The algebraic mixing length model proposed by Patankar (1979) is adopted in the present study. The model takes account of the proximity of both the fin surfaces and tube wall as well as of the gradients in the radial and circumferential directions. Since the available wall functions of the standard k-ϵ model account for the influence of only single wall, they are not suitable for the present problem, where the influences of both the tube wall and the fin surface are important near the fin region (Figure 1). The resultant mixing length l is calculated by

$$\frac{1}{l} = \frac{1}{l_{\mathrm{p}}} + \frac{1}{l_{\mathrm{c}}} \quad (6)$$

where l_{p} is the mixing length considering a pipe flow without fins, l_{c} is the mixing length if the inter-fin surface is likened to a parallel plate channel (Patankar, 1979). Equation (6) was employed to evaluate the mixing length at all points in the inter-fin space.

Equations (2–5) are completed by the following set of boundary conditions:

$$\text{for } \theta = 0 \text{ or } \theta = \frac{2}{3}\pi: \quad u = 0,\ v = 0,\ w = 0,\ \frac{\partial t}{\partial \theta} = 0; \quad (7a)$$

$$\text{for } r = r_{\mathrm{i,ic}} \text{ or } r = r_{\mathrm{o,oc}}: \quad u = 0,\ v = 0,\ w = 0,\ \frac{\partial t}{\partial r} = 0 \text{ (Figure 1)}; \quad (7b)$$

$$\text{for } x = 0: \quad t = t_{\mathrm{in}},\ v = 0,\ w = 0,\ u = u_{\mathrm{in}}(j),\ j = 1, 7 \text{ (Figure 1)}; \quad (7c)$$

Since there is no reverse flow in the main flow direction, and the diffusion of momentum, heat is negligible in that direction, the downstream pressure field has little influence on the upstream flow conditions. It is this convenient behavior of the boundary-layer flows that enable us to employ a marching integration from an upstream station to a downstream one. This procedure can be regarded as a boundary-layer method.

Note that in equations (4a) $\bar{p}$ can be thought of as a form of space-averaged pressure over a cross section, and $\tilde{p}$ in Equations (4b) and (4c) is the small pressure variation governing the flow distribution in the cross-section. The gradient $\partial\bar{p}/\partial x$ is supposed to be known (or calculated) before we proceed to

get the lateral pressure gradient $\partial\tilde{p}/\partial\theta$ and $\partial\tilde{p}/\partial r$. In the confined flow, we regard $\partial\bar{p}/\partial x$ as uniform over a cross-section and then obtain it from the integral mass-conservation eqs(Patankar, 1972). Here an assumption is made as follows:

$$p = \bar{p} + \tilde{p} \tag{8a}$$

$$\frac{\partial p}{\partial x} = \frac{\partial \bar{p}}{\partial x}, \quad \frac{\partial p}{\partial \theta} = \frac{\partial \tilde{p}}{\partial \theta}, \quad \frac{\partial p}{\partial r} = \frac{\partial \tilde{p}}{\partial r} \tag{8b}$$

Such an assumption de-couples the longitudinal and the lateral pressure gradients, which may be calculated in a different way. In this paper, the pressure field is determined by: first calculating an intermediate velocity field based on an estimated pressure; and then obtaining appropriate correction so as to satisfy the continuity equation. This kind of treatment to pressure is necessary to make the equations parabolic, resulting in the freedom to solve a three-dimensional problem with a two-dimensional computer storage, even though the flow is three-dimensional and the full equations are elliptic. The details of solution procedures can be found in the method proposed by Patankar (1972). Lin *et al.* (1995) presented an example of usage of the marching procedure, which solved the developing flow and heat transfer in annular-sector ducts.

3. Numerical procedure

The above governing equations were discretized by the finite volume approach. The convection term in the cross-section is approximated by the power law scheme. The velocity field of the cross-section were solved by an elliptic solver, using SIMPLE algorithm to deal with the coupling between velocity and pressure field. While the governing eqsof the axial velocity was discretized by one-sided scheme with an assumed axial pressure drop. The computation of one-step forward was considered converged if the axial mass flow rate balance meets the required accuracy. The details of this computation procedure may be found in Patankar (1972). Here we focus our presentation on the detailed procedure for obtaining an appropriate flow distribution at the channel inlet and revealing the conjugated character between the solid fuel layer and the cooling water. The solution procedure for the velocity and temperature fields in the subchannels and solid regions is as follows:

(1) Assuming the inlet velocity distribution for the seven ducts, according to the given total flow rate.

(2) Solving the velocity distribution field for the annular-sector ducts separately. The fluid thermophysical properties are determined by the locally averaged temperature, determined from energy balance equation.

(3) Updating the inlet velocities for the seven channels, according to the computed pressure drops in each channel.

(4) Going back to step 2 until the following criterion for the pressure drops is satisfied.

$$\frac{|\Delta p(j)_{j=1,7} - \Delta p_{\text{mean}}|_{\max}}{\Delta p_{\text{mean}}} \leq 3\% \tag{9}$$

where Δp_{mean} is the average value of pressure of the seven channels.

(5) Calculating the temperature field for the entire region, including annular-sector channels, uranium layers, aluminum layers, fins and inner and outer casings.

(6) The above procedures, from step 2 to step 5, is repeated so that the fluid physical properties are updated by the introduction of the newly solved temperature distribution field. The iteration stops when the required convergence criteria are satisfied.

A careful grid-independence study was carried out to ensure that results are basically independent of grid system. For this purpose, three grid systems $20(r) \times 98(\theta) \times 30(x)$, $30(r) \times 136(\theta) \times 40(x)$, $40(r) \times 156(\theta) \times 50(x)$ are tested. It is found that for most cases examined, the maximum relative error in the velocity and temperature solutions between grid systems $30 \times 136 \times 40$ and $40 \times 156 \times 50$ is within 1.5 per cent. Therefore, the accuracy of the solution from the $30 \times 136 \times 40$ grid system is thought to be satisfactory, and it is employed in all computations.

For the longitudinal pressure gradient, the following convergence criterion is enforced:

$$\left| \frac{\dfrac{\partial \bar{p}^{n+1}}{\partial x} - \dfrac{\partial \bar{p}^{n}}{\partial x}}{\dfrac{\partial \bar{p}^{n}}{\partial x}} \right| \leq 1 \times 10^{-5} \tag{10}$$

At each marching step, the convergence criteria for stopping iteration in elliptic computation is as follows:

$$\left| \frac{\Phi^{n+1} - \Phi^{n}}{\Phi^{n}} \right| \leq 1 \times 10^{-5} \tag{11}$$

where ϕ denotes v, w.

The local heat transfer coefficients $h(x)$ and the Nusselt numbers $\text{Nu}(x)$ for the seven channels are obtained by

$$h_j(x) = \frac{q_j(x)}{t_{w,j}(x) - t_{b,j}(x)} \quad Nu(x) = \frac{h_j(x) \cdot D_j}{k} \quad j = 1 - 7 \tag{12}$$

where $q_j(x)$ is the local heat flux, $t_{b,j}(x)$ and $t_{w,j}(x)$ are the local bulk temperature and wall temperature respectively. $t_{b,j}(x)$ is calculated from

$$t_{b,j}(x) = \frac{\int_0^{\frac{2}{3}\pi} \int_{r_{o,j}}^{r_{i,j+1}} utrdrd\theta}{\int_0^{\frac{2}{3}\pi} \int_{r_{o,j}}^{r_{i,j+1}} urdrd\theta} \quad (13)$$

where $r_{o,j}$ and $r_{i,j+1}$ are the outer and inner radius of each water channel.

The channel averaged Nusselt number is defined as

$$Nu_{m,j} = \frac{\int_0^L Nu_j(x)dx}{L} \quad (14)$$

4. Results and discussion

Computations were performed first for a basic case with $t_{in} = 50^{\circ}C$, $F = 16.1\,kg/s$ and $q_{max} = 1.188 \times 10^{10}\,W/m^3$. Then parametric studies were conducted by changing water inlet temperature and inlet velocity, from 20°C to 80°C and 6 m/s to 15 m/s, respectively. The presentation will start from the flow and heat transfer characteristics of the basic case, followed by the effects of the inlet temperature and velocity on the maximum surface temperature.

4.1 Flow velocity distribution

As mentioned above, at a given total flow rate, flow velocity distribution among different channels is adjusted according to the same pressure drop principle. Table II presents the results of the inlet average velocity distribution.

Some important observations can be made from the table. First, the inlet velocities of the two bilateral channels are apparently lower than those of the middle. Secondly, among the five middle channels, the average inlet velocity increases slightly from inner to outer. The observations can be understood from the effects of viscosity, velocity and equivalent diameter on pressure drop. It is well known that pressure drop for a channel will increase with the increase of the viscosity and velocity of the water, while it will decrease with the

Table II. Channel-averaged inlet velocities for the channels under identical pressure drop

Channel number	1	2	3	4	5	6	7
Averaged inlet velocity (m/s)	9.558	10.108	10.173	10.191	10.201	10.207	9.533

increase of the channel equivalent diameter. Water in the two bilateral channels is heated by one-side wall, with the other wall insulated. This fact results in a lower water temperature and hence a higher viscosity than the water in the middle channels. Therefore, to keep the same pressure drop as the others, the bilateral channels should have smaller inlet velocities. On the other hand, the five middle channels were heated by two-side walls, they should have higher inlet velocities comparing to the two bilateral channels mainly due to their high water temperature. The small difference in the inlet velocity among the five channels came from their different equivalent diameters.

4.2 Temperature Distribution

Figures 2–4 show the variations of the local bulk temperature of water in the seven channels, uranium layers and aluminum layers (including the inner and outer casings), respectively, with the axial distance. Apart from seven water cooled channels, there are six uranium layers and fourteen aluminum layers. We group the aluminum layers into two classes, outer aluminum layers and inner aluminum layers, according to their relative position to the channels to which they are close. For a better understanding of the different positions of the numbered objects, the four numbering systems are shown in Figure 1. It can be seen from Figure 2 that the water temperature in the two bilateral channels is much lower than that of the others. Figure 3 shows that the uranium temperature of the first layer is much lower than those of the others because of its better cooling condition, while the temperature of the sixth uranium layer, although still lower than the values of the other four layers, is a bit higher than that of the first one. This is basically because of the lower convective heat transfer coefficient of the Channel 7, which will be presented in later discussion. The aluminum layer temperature distributions presented in

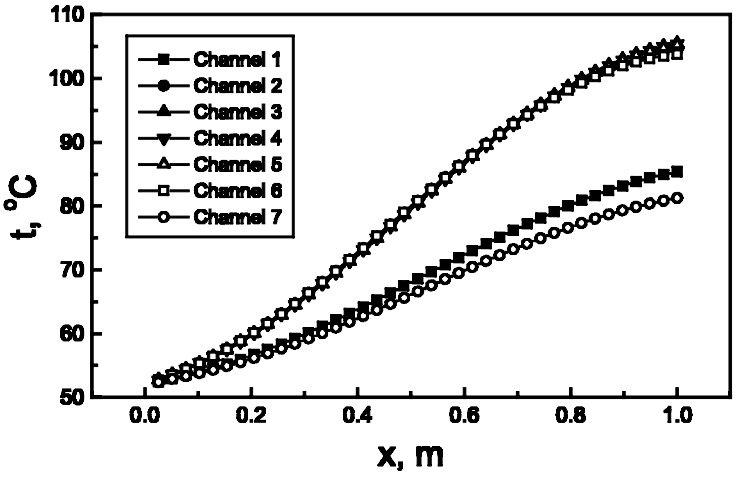

Figure 2.
Local bulk temperature of water along the axial direction

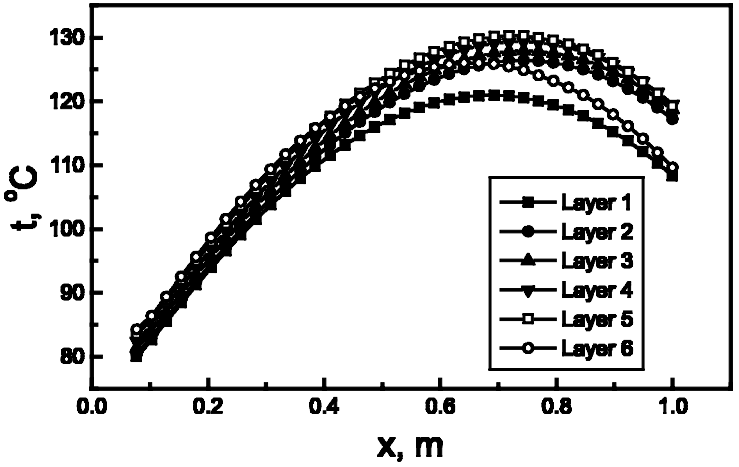

Figure 3.
Local bulk temperature of uranium layers along the axial direction

Figure 4 indicates a similar variation pattern as that of uranium, that is, the first inner aluminum layer and the seventh outer one have the lowest temperature at each cross-section, while the fifth outer aluminum layer and the sixth inner layer possess the highest temperatures. To sum up, the temperature of the fifth uranium layer and the related aluminum layers are the highest. Thus for the safe operation of the reactor, more attention should be paid to the temperature situation of the fifth uranium layer.

It is interesting to note that from Equation (1), the highest volume heat source occurs at the axial location of $x = 0.5$ m where sine function equals 1 and $q(x) = q_{\max}$. However, all the temperature distribution patterns shown in Figures 3 and 4 exhibit their summit at the location around $x = 0.7-0.8$ m rather than 0.5 m, showing some delay between the distributions of volumetric heat source and the temperature in uranium layer. This is also a noticeable feature for the design and operation of such kind of reactor.

Figure 5 presents the local maximum surface temperature for fourteen aluminum layers along the axial direction, which shows the similar characteristics to the curves shown in Figure 4.

Attention is now turned to the temperature distribution at the cross-sections in different axial location. Take channel 2 as a representative for the middle channels. Its temperature contours are shown in Figure 6 for four axial locations. Two features may be noted from the figure. First, in each of the temperature contour of the four cross-sections, there is a core region in which the water temperature is more or less uniform. The radian span of this core region decreases with the increase of axial location, indicating the development of the thermal boundary layer along the flow direction. Second, the temperature gradients normal to the inner and outer circular surfaces in the center region of the peripheral direction are much greater than those in the two end regions near

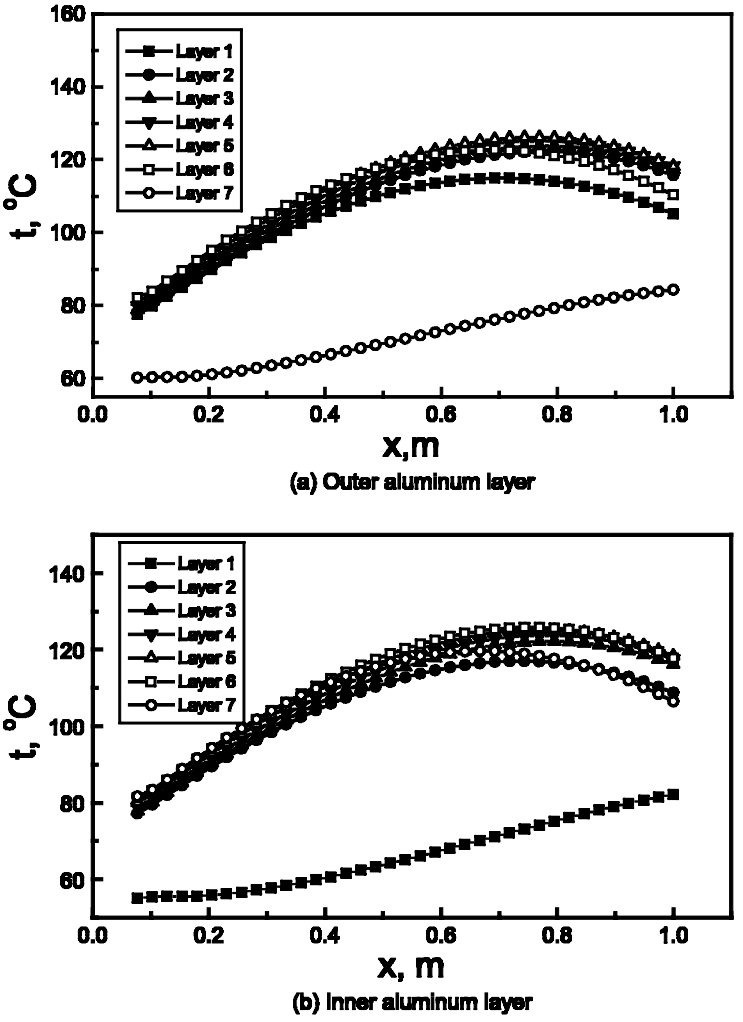

Figure 4.
Local bulk temperature of aluminum layers along the axial direction

the fins in each cross-section. This implies that the local convective heat transfer coefficient of the center region is much higher than those of the two ends. This will lead to non-uniform peripheral surface temperature distribution of each channel. To have a better understanding for this non-uniformity, Figure 7 provides the peripheral temperature for channel 2 at $x = 0.795$ m. It can be seen clearly that the end temperatures are significantly higher than their counterpart in the center region, the difference ranging from 10°C to 15°C for the parameters studied in this paper. This is also a noticeable character for the design and operation of such kind of reactor.

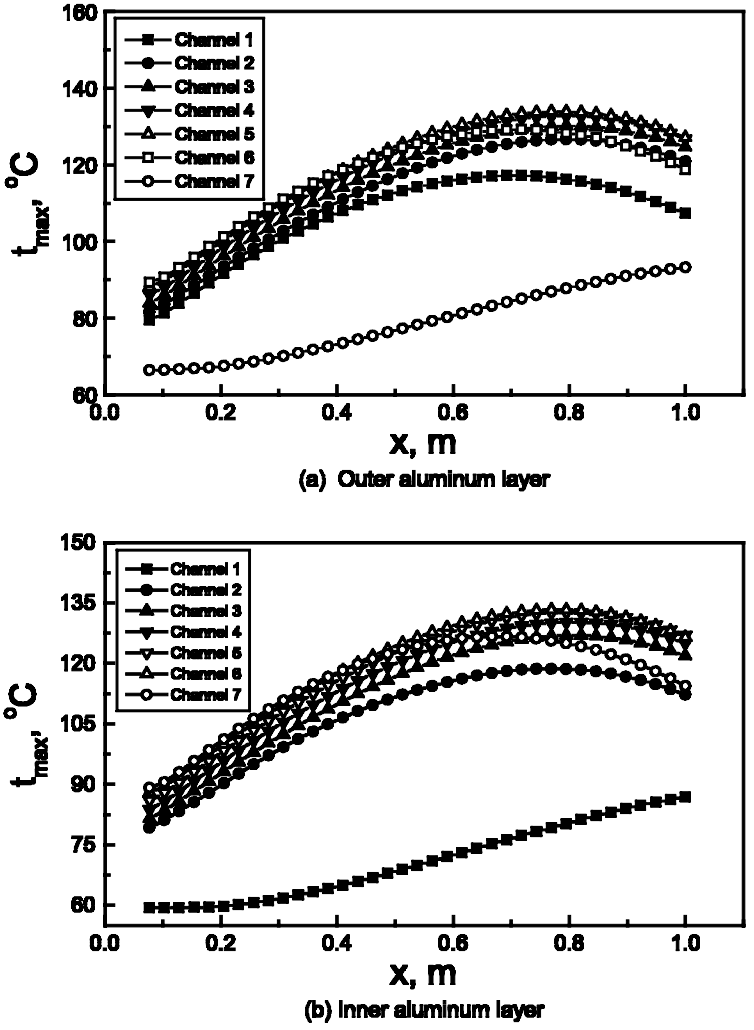

Figure 5.
Local maximum surface temperature for aluminum layers along the axial direction

4.3 Heat transfer

Heat transfer coefficient distribution is of great importance in the present application. Figure 8 represents the axial variation of the local heat transfer coefficient for the seven channels. As seen from the figure, all the curves do not approach to a constant value with the increase of axial location. This is resulted from the non-uniform axial heat flux distribution (Equation (1)). For the middle channels which are heated by both the inner and outer walls, the local heat transfer coefficient increases to a maximum value at certain locations and then decreases monotonically. While for the one-wall-heated bilateral channels, the local heat transfer coefficient exhibits the entrance problem character at the

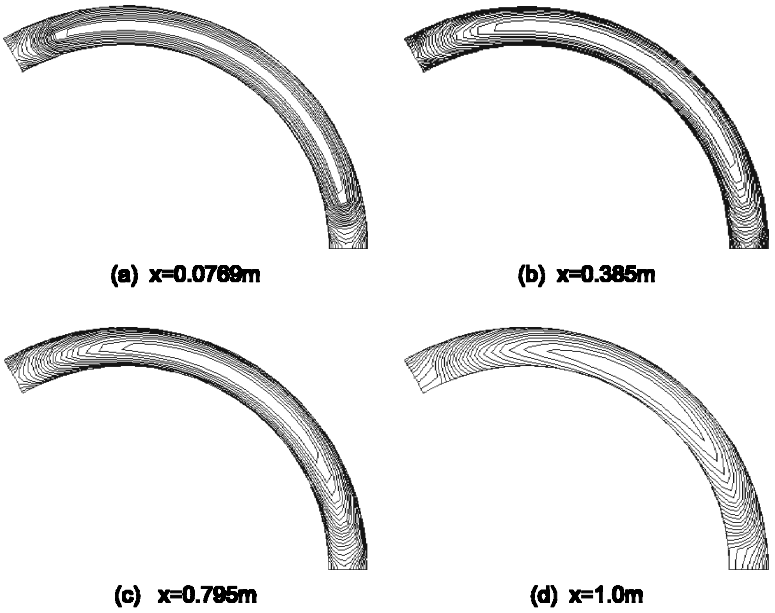

Figure 6.
Isothermos at different channel cross-sections for Channel 2

very beginning of the channel, and then takes the variation pattern of the middle channel heat transfer coefficient, with about 30–40 per cent percentage reduction in the absolute value.

The effect of the Reynolds number on the averaged Nusselt number is presented in Figure 9. It can be noted that the bilateral walls also exhibit a

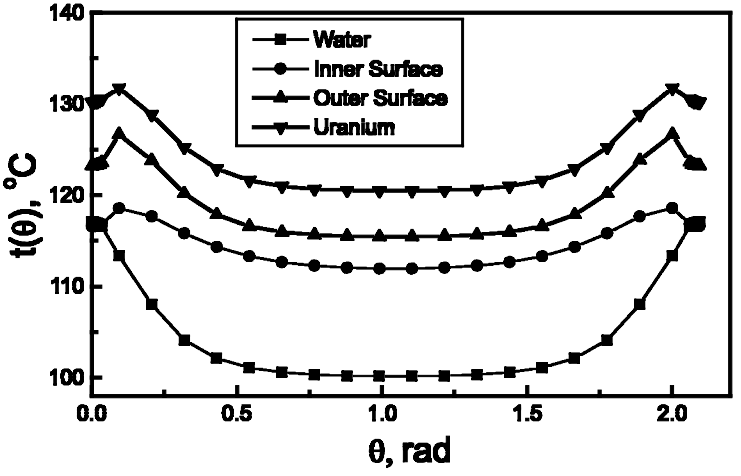

Figure 7.
Temperature distribution along the peripheral direction for Channel 2 at $x = 0.795$ m.

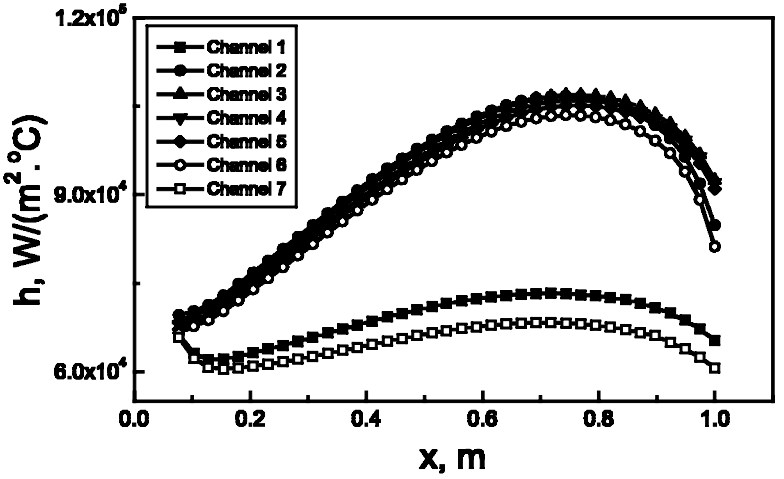

Figure 8.
Local heat transfer coefficients along the axial direction

different characteristic from the middles. At the same Reynolds number, the averaged Nusselt numbers of Channel 1 and Channel 7 are higher than those of the others, which seems to be contradictory to Figure 8. It should be noted that in Figure 8 the water viscosities of Channel 1 and Channel 7 are much higher than those of other channels due to their lower temperatures and their velocities are lower (Table II). Therefore the Reynolds numbers in the bilateral channels 1 and 7 are lower than that of the middles (Channels 2 to 6). In the meantime, at the same Reynolds number, the Nusselt numbers of the relatively outer channels are a little smaller than that of the inner ones.

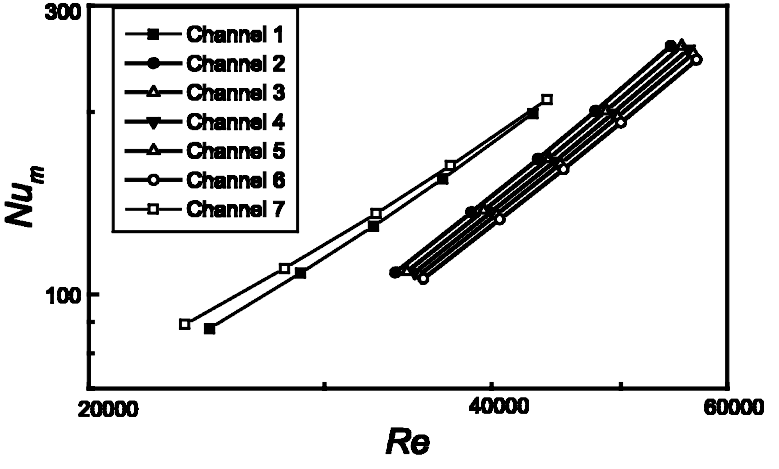

Figure 9.
Variation of the averaged Nusselt number with Reynolds number

4.4 Effects of the inlet water temperature and velocity

Since temperature distribution is the major concern of the present study, the computational results for the extended parameters of the inlet water temperature and inlet velocity are provided for the effects on the maximum channel surface temperature (so-called hot spot temperature) and the maximum uranium temperature. Figure 10 presents the numerical results. It should be noted that when the effect of one parameter is examined, all other parameters remain the same as for the basic case. From Figure 10(a), an almost linear

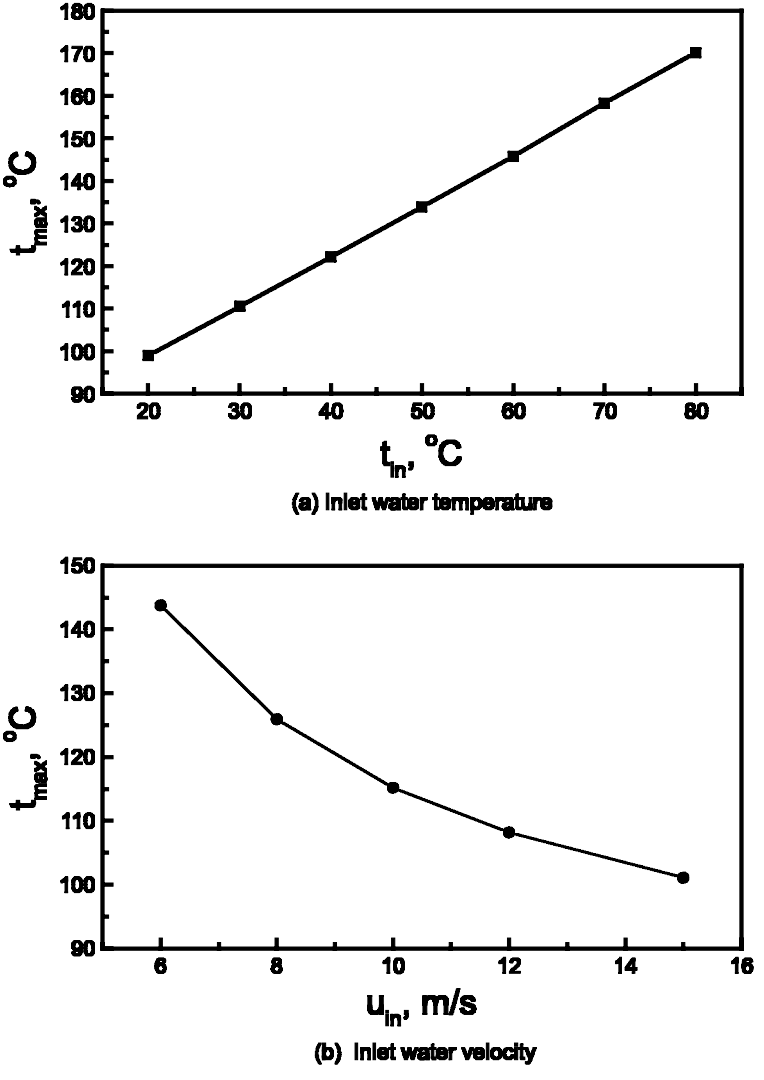

Figure 10.
Variation of maximum temperature with inlet water temperature and velocity

variation of the maximum surface temperature with the inlet temperature may be observed. This is an expected outcome, since the variation of the wall temperature is not large enough to make an appreciable change of the convective heat transfer coefficient. Thus with the same heat flux, the local temperature difference between wall and water remains the same, resulting the linear variation of the wall temperature with water. Figure 10(b) shows that the maximum temperature of the aluminum surface and the uranium decrease with the increase of inlet velocity. The curves shown in the figure exhibit somewhat asymptotic character when inlet velocity goes quite high (from 6 to 15 m/s). This is because that the heat transfer resistance from the uranium to the water mainly lies in the solid conduction when the surface convective heat transfer coefficient exceeds some specific values. Therefore, the increase of water inlet velocity will decrease the wall temperature efficiently only when the water-side heat transfer resistance is predominated.

It should be noted that all the temperature all the computations presented in the present paper are for the ideal case. This means that the factors which lead to the additional heat transfer resistances are not taken into account. These factors include the thin water film between the aluminum surface and the space (fin), the oxidization of the aluminum surface and the distortion of the uranium layers. The computational results are compared with the experimental data given by Chen and Jiang (1984) in the case of $t_{in} = 34.98℃$, $F = 15.7\,kg/s$ and $q_{max} = 1.001 \times 10^{10}\,W/m^3$ in the presence of the above effects. The water film and the oxidized aluminum coating had the thickness of 0.5 mm and 0.05 mm respectively, while the uranium distortion was 0.125 mm thick. Table III shows the results. It can be found that after considering the effects of water film, oxidized aluminum coating and the uranium distortion, a good agreement between numerical and experimental results is achieved, with the maximum deviation about 14 per cent. This agreement indicates that the present numerical approach can be used to predict the fluid flow and temperature filed of the multi-channel fuel elements.

Point	Channel	Position	Experimental data (℃)	Computational results (℃)	Deviation (per cent)
1	2	x = 0.70 m	123.38	112.58	8.7
2	3	x = 0.70 m	114.78	108.60	5.4
3	4	x = 0.70 m	114.05	113.57	0.4
4	5	x = 0.75 m	131.72	119.34	9.4
5	6	x = 0.70 m	110.11	124.01	12.6
6	4	x = 0.65 m	130.58	112.25	14.0
7	4	x = 0.75 m	113.99	114.35	0.3
8	5	x = 0.70 m	126.48	119.18	5.8
9	5	x = 0.70 m	127.05	119.17	6.2

Table III. Comparison between experimental and computational results

5. Conclusions

Three-dimensional parabolic turbulent forced convection heat transfer and fluid flow characteristics in multi-channel, narrow-gap fuel element, with non-uniform heat flux, are studied numerically. The boundary-layer method with a mixing length turbulent model was proved to be able to simulate the flow and pressure characteristics in the multi-channels. The main conclusions are:

(1) The inlet velocities of the bilateral channels are apparently lower than those of the middle, and among the five middle channels, the average inlet velocity is almost the same with very slight increase from inner to outer.

(2) Because of the non-uniform heat flux, axial local heat transfer coefficients for the seven channels don't approach fully developed constant value.

(3) For both aluminum and uranium layers, the local temperature distribution along axial coordinate is of sinuous type, with the peak at $x = 0.7-0.8$ m. Their maximum temperature occurs in the fifth uranium layer.

(4) At each cross-section, the periphery temperature distribution is not uniform, rather the temperature of the two ends are appreciably higher than those of the center region.

(5) At the same Reynolds number, the averaged Nusselt numbers of water in Channel 1 and Channel 7 are higher than those of the middles. And among the five middle channels, the Nusselt number for the relatively outer channel is a little smaller than the inner one at the same Reynolds number.

(6) The maximum surface temperature increases almost linearly with the inlet water temperature, while decrease almost asymptotically with the inlet average velocity.

References

Chen, D.L. and Jiang, F. (1994), "Flow and temperature measurement for fuel element in HFETR", *Nuclear Science and Engineering*, Vol. 4 No. 2, pp. 178-82 (in Chinese).

Hanjalic, K. (1994), "Advanced turbulence closure models: a review of current status and future prospects", *Int J Heat Mass Transfer*, Vol. 15 No. 3, pp. 178-203.

Lin, M.J., Tao, W.Q. and Lue, S.S. (1995), "Study on friction factor of developing and developed laminar flow in annular-sector ducts", *J Thermal Science*, Vol. 4 No. 3, pp. 180-84.

Lin, M.J., Wang, Q.W. and Tao, W.Q. (2000), "Developing laminar flow and heat transfer in annular-sector duct", *Heat Transfer Engineering*, Vol. 21, pp. 53-61.

Nida, T. (1980), "Analytical solution for the velocity distribution laminar flow in an annular-sector duct", *International Journal of Chemical Engineering*, Vol. 20, pp. 258-65.

Patankar, S.V. and Spalding, D.B. (1972), "A calculation procedure for heat, mass and momentum transfer in 3-D parabolic flows", *Int. J. Heat Mass Transfer*, Vol. 15, pp. 1787-1806.

Patankar, S.V., Ivanovic, M. and Sparrow, E.M. (1979), "Analysis of turbulent flow and heat transfer in Internally Finned Tubes and Annuli", *ASME J of Heat Transfer*, Vol. 101, pp. 29-37.

Ramdhyani, S. (1997), "Two-equations and second-moment turbulence models for convective heat transfer", in, *Advances in Numerical Heat Transfer*, Minkowycz, W.J., Sparrow, E.M. (Eds), Vol. 11 pp. 171-99.

Soliman, H.M. (1987), "Laminar heat transfer in annular sector ducts", *ASME J Heat Transfer*, Vol. 109, pp. 247-9.

Sparrow, E.M., Chen, T.S. and Jonson, V.K. (1964), "Laminar flow and pressure drop in internally finned annular ducts", *Int. J. Heat Mass Transfer*, Vol. 7, pp. 583-5.

Wang, J.F. (1981), "Thermal performances of multi-casing fuel element with fins in HFETR", *Nuclear Power Engineering*, Vol. 2 No. 3, pp. 50-5 (in Chinese).

Yu, E.J. (1981), "Computational prediction of the hot point temperature in multi-casing fuel element", in, *Computations and experiments on thermal engineering in nuclear reactor*, Nuclear Power Press, Beijing pp. 35-41.